Interactions between Increasing CO_2 and Antarctic Melt Rates

SHONA MACKIE AND INGA J. SMITH

Department of Physics, University of Otago, Dunedin, New Zealand

DAVID P. STEVENS

School of Mathematics, University of East Anglia, Norwich, United Kingdom

JEFF K. RIDLEY

Met Office, Exeter, United Kingdom

PATRICIA J. LANGHORNE

Department of Physics, University of Otago, Dunedin, New Zealand

(Manuscript received 26 November 2019, in final form 14 July 2020)

ABSTRACT

Meltwater from the Antarctic ice sheet is expected to increase the sea ice extent. However, such an expansion may be moderated by sea ice decline associated with global warming. Here we investigate the relative balance of these two processes through experiments using HadGEM3-GC3.1 and compare these to two standard idealized CMIP6 experiments. Our results show that the decline in sea ice projected under scenarios of increasing CO_2 may be inhibited by simultaneously increasing melt fluxes. We find that Antarctic Bottom Water formation, projected to decline as CO_2 increases, is likely to decline further with an increasing meltwater flux. In our simulations, the response of the westerly wind jet to increasing CO_2 is enhanced when the meltwater flux increases, resulting in a stronger peak wind stress than is found when either CO_2 or melt rates increase exclusively. We find that the sensitivity of the Antarctic Circumpolar Current to increasing melt fluxes in the Southern Ocean is countered by increasing CO_2, removing or reducing a feedback mechanism that may otherwise allow more heat to be transported to the polar regions and drive increasing ice shelf melt rates. The insights presented here and in a companion paper (which focuses on the effect of increasing melt fluxes under preindustrial forcings) provide insights helpful to the interpretation of both future climate projections and sensitivity studies into the effect of increasing melt fluxes from the Antarctic ice sheet when different forcing scenarios are used.

KEYWORDS: Antarctica; Sea ice; Southern Ocean; Climate models; Coupled models

1. Introduction

Meteoric ice from Antarctica flows through the grounding line of the ice shelves and either melts from the ice shelf bases into the ocean or calves from the ice shelf fronts as icebergs that are transported and melt. Sublimation and surface runoff are small compared to the rates of mass loss through icebergs and ice shelf melt in the Antarctic (Liston and Winther 2005). The meltwater that enters the ocean is fresh and therefore buoyant, and so it can drive a stratification that inhibits mixing and prevents warm deeper waters from influencing the surface, promoting sea ice production and inhibiting sea ice basal melt (Bintanja et al. 2015; Mackie et al. 2020b). This contrasts with the effect of increasing CO_2, which has a warming effect that inhibits sea ice production. Sea ice is more reflective than the ocean surface, and so changes in sea ice cover represent changes to the

Denotes content that is immediately available upon publication as open access.

Supplemental information related to this paper is available at the Journals Online website: https://doi.org/10.1175/JCLI-D-19-0882.s1.

Corresponding author: Shona Mackie, shona.mackie@otago.ac.nz

DOI: 10.1175/JCLI-D-19-0882.1

planetary albedo and affect Earth's radiation budget through the temperature–albedo feedback (Rind et al. 1995), with potential implications for almost all aspects of climate. Furthermore, by creating a physical barrier between the ocean and atmosphere, sea ice alters the amount of precipitation reaching the ocean. This has implications for local ocean salinity, which is further affected by brine rejection associated with sea ice production, and surface freshening associated with sea ice melt (Weeks 2010). Changes to ocean salinity from these processes can impact ocean density differences that drive much ocean circulation (Bromwich et al. 1998). The insulating effect of sea ice can also result in a locally warmer ocean and cooler atmosphere as less heat is transferred from the former to the latter (Andreas and Murphy 1986; Bromwich et al. 1998; Bronselaer et al. 2018; Mackie et al. 2020b). Changes to sea ice cover, driven by the competing effects of increasing CO_2 and increasing melt fluxes from Antarctica, can therefore result in ocean and climate changes that extend beyond the sea ice edge, and require appropriate representation in climate models.

Increases in CO_2 are generally included in calculations of the likely future climate; however, increases in the rate at which meteoric ice is lost from Antarctica are generally not considered (i.e., the rate is assumed constant), or are underestimated compared to glaciological estimates. This study builds on a parallel study, which looked at the effect of increasing melt rates, and considers where the effect of an increasing meltwater flux may enhance or reduce some climate effects attributable to increasing levels of CO_2.

An increase in meteoric ice melt fluxes entering the Southern Ocean results in a cooling of the ocean surface, increased sea ice cover, and a colder lower atmosphere. Such a shift in the thermodynamics results in a northward shift of the meteorological polar front, the boundary between the air masses of the polar cell and the Ferrel cell, and of the intertropical convergence zone (ITCZ) (Bronselaer et al. 2018; Mackie et al. 2020b). An increase in meltwater causes a surface freshening, potentially reducing the meridional density gradient (Mackie et al. 2020b), which is a driver for the Antarctic Circumpolar Current (ACC) (Russell et al. 2006). The ACC is related to the amount of heat transported from the low- to high-latitude ocean, and changes in its strength may therefore affect ice shelf melt by influencing the heat that reaches the ice shelf fronts. Stratification can inhibit deeper waters from rising to the surface to exchange heat and gas with the atmosphere. Via this mechanism, an increase in melt fluxes can cause midlayer ocean waters to warm (Bronselaer et al. 2018; Mackie et al. 2020b). If the meltwater enters at depth along the ice shelf fronts, then it can become supercooled as it rises to the surface, forming frazil ice crystals in the water column that rise to the surface to form new sea ice, or attach to the underside of existing sea ice, enhancing sea ice growth (Weeks 2010; Mackie et al. 2020b). If the volume of the melt entering the ocean at depth is high enough, then this rising water can drive a local overturning (Merino et al. 2018), and a freshening of the whole water column that inhibits the formation of Antarctic Bottom Water (AABW) (Mackie et al. 2020b). AABW is usually formed as dense saline water, created by brine rejection during sea ice production at some key locations, sinks from the surface to the continental shelf, from where it spills over to fill the deep ocean basins. AABW formation constitutes the southern end of the thermohaline circulation, which is an important mechanism by which heat is distributed around the planet (Weaver et al. 2003; Sloyan 2006; Marsland et al. 2007). As the upper ocean warms and its density decreases with increasing levels of CO_2, AABW formation is anticipated to reduce, and this reduction could be enhanced by the decrease in AABW that is driven by the simultaneously increasing melt fluxes. It is important that any change to AABW formation is represented realistically in climate models in order for reliable projections to be made of high-southern-latitude ocean properties and circulation.

Previous works have found the position and strength of the westerly winds around Antarctica, driven by the latitudinal temperature gradient in combination with the planetary rotation, to be impacted by Antarctic sea ice extent (Kidston et al. 2011; Mackie et al. 2020b). The circumpolar winds are associated with midlatitude weather in the Southern Hemisphere (Hoskins and Hodges 2005; Le Quéré et al. 2007), and are anticipated to strengthen and to shift to higher latitudes under future climate warming (Bracegirdle et al. 2013). This raises the question of whether their sensitivity to sea ice extent could be enhanced in a warming climate. We consider whether sea ice changes, driven by increasing melt fluxes, could offset or compound the changes to the westerlies that are attributable to rising temperatures.

The latest generation of HadGEM in the global coupled configuration, HadGEM3-GC3.1, includes several improvements to the representation of sea ice and ocean processes (Ridley et al. 2018; Storkey et al. 2018), including a realistic spatial distribution of ice shelf melt from Rignot et al. (2013), a new parameterization for ice shelf basal melt (Mathiot et al. 2017), and explicit representation of icebergs (Marsh et al. 2015). However, in common with most climate models, the rate of mass loss from the Antarctic continent remains constant, and climate projections submitted to the CMIP6 experiment are calculated on this basis. In reality, the rate of mass

loss is known to be increasing for at least some ice shelves (Rignot et al. 2008; Sutterley et al. 2014; Martín-Español et al. 2016; Shepherd et al. 2018), and it is likely that further increases will occur as the climate warms in future (Timmermann and Hellmer 2013). Studies into the sensitivity of climate models to this assumption have shown that impacts on sea ice and ocean processes are likely, but different results have been found in different works, for example Richardson et al. (2005), Turner et al. (2013), Bintanja et al. (2013, 2015), Zunz and Goosse (2015), Swart and Fyfe (2013), Pauling et al. (2016, 2017), Merino et al. (2018), and Bronselaer et al. (2018). The modeling advances included in HadGEM3-GC3.1 make it appropriate to revisit this question and investigate the impact of increasing rates of Antarctic mass loss for climate projections made using this model.

Reliable projections of global climate require sea ice and ocean processes to be appropriately represented in climate models, and so it is important to consider the impact that increasing Antarctic melt rates may have on these, and whether these could enhance or inhibit effects attributable to CO_2-induced warming. We investigate the behavior of these characteristics in the CMIP6 model HadGEM3-GC3.1. In the accompanying paper, the effects of increasing rates of iceberg and ice shelf melt are reported assuming external greenhouse gas forcings to be fixed at preindustrial levels (Mackie et al. 2020b). Here, we evaluate whether these same sensitivities occur in an environment where CO_2 increases simultaneously with the melt rate (both are applied as external forcings), and assess whether the sensitivity of some ocean and sea ice processes to an increasing melt rate could enhance, or partially counter, the effects of CO_2-induced warming.

2. Method

a. Model description

HadGEM3-GC3.1 (Williams et al. 2018; Kuhlbrodt et al. 2018) is the coupled land–ocean–sea ice–atmosphere model that forms the physical core of the U.K. Earth System Model, and is the basis from which the New Zealand Earth System Model is being developed (Williams et al. 2016). It uses GA7-GL7 for the atmosphere and land (Walters et al. 2019), GO6 for the ocean (Storkey et al. 2018), and GSI8.1 for the sea ice component (Ridley et al. 2018). For this work, we use the ORCA1 grid (nominally 1° resolution) for the ocean and sea ice, and a resolution of 1.875° × 1.25° for the atmosphere. The ocean is configured with 75 vertical layers, and the atmosphere with 85 layers. Mass loss from Antarctica in the standard configuration of the model is kept constant at a rate of 1770.75 Gt yr^{-1} (set so as to maintain the ice sheets in mass balance under preindustrial forcings). Excepting a small amount of accumulation that melts or sublimates at the surface (according to atmospheric conditions over Antarctica), the mass loss is distributed around the coastal ice shelves following the distribution in Rignot et al. (2013). Forty-five percent of the mass flux at each ice shelf constitutes an iceberg calving flux, wherein icebergs are created following the size distribution from Bigg et al. (1997). Icebergs travel and melt according to ocean surface properties, following the Lagrangian scheme in Marsh et al. (2015), with a cooling effect on the surface ocean from the melt due to the latent heat. The remaining 55% of the mass flux represents ice shelf basal melt, which is distributed vertically between the average grounding line depth and the base of the ice shelf at its front, according to the parameterization in Mathiot et al. (2017) (the cavity is not explicitly represented). The rate of mass loss from the Greenland Ice Sheet is also assumed constant, and similar processes are followed, but with a calving rate of 100% since there are assumed to be no ice shelves.

b. Experiments

Two standard HadGEM3-GC3.1 CMIP6 simulations, the preindustrial control (PIControl) and the 1% yr^{-1} increasing CO_2 (CO2), provide the reference experiments for this study. Note that in the CMIP6 1% CO_2 simulation, CO_2 reaches 4 times preindustrial levels after 140 years, but CO2 comprises only the first 100 years of this simulation. We undertake additional simulations, intended to assess the effect of an increasing rate of mass loss from Antarctica relative to PIControl (mass loss from the Greenland Ice Sheet remains as per the standard model in all experiments). The first experiment, FW, investigates the sensitivity of the modeled ocean and sea ice to an increasing rate of total mass loss from the Antarctic continent, and is discussed in Mackie et al. (2020b). All external forcings in FW (except Antarctic mass loss) are held constant at preindustrial levels. In the second experiment, FWCO2, CO_2 increases by 1% annually, as for the reference simulation, CO2, and the same increase in Antarctic mass loss is applied as for FW (both the mass loss and the CO_2 are prescribed as external forcings, and so are not coupled to each other in FWCO2). All other external forcings are held constant. FWCO2 addresses two questions: first, whether the sensitivities found in FW for a preindustrial world also apply in a world with increasing CO_2, and second, whether the effect of the additional meltwater could counter, or enhance, effects attributable to increasing CO_2. In FW and FWCO2, the increased mass loss is

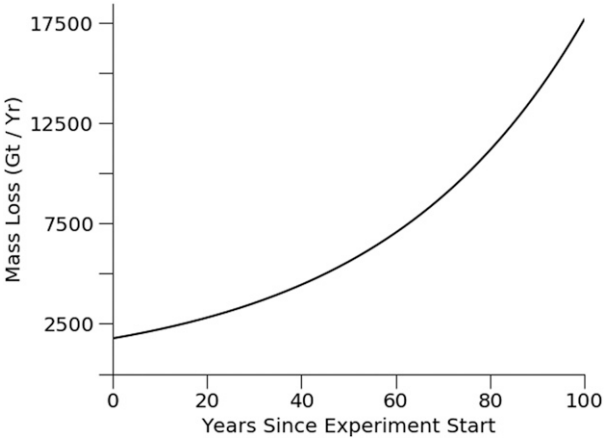

FIG. 1. The total rate of meteoric ice mass loss from the Antarctic continent used for FW and FWCO2.

distributed spatially around the continent, and proportioned between ice shelf basal melt and an iceberg calving flux, as for the standard model. The total rate of mass loss in FW and FWCO2 is increased by 2.33% each year for 100 years, so that the rate of mass loss after 100 years is 10 times the initial rate (Fig. 1). The scenario was designed to look at the sensitivity of the modeled ocean and sea ice to the increasing rate of mass loss, rather than to be realistic in terms of absolute numbers. For context, the freshwater contribution from Antarctica to the Southern Ocean could rise above 1 Sv ($1\,\text{Sv} \equiv 10^6\,\text{m}^3\,\text{s}^{-1}$ so this is $31\,104\,\text{Gt}\,\text{yr}^{-1}$ using HadGEM3-GC3.1's 360-day model year) by the year 2100 under RCP 8.5 (DeConto and Pollard 2016), which is almost twice the maximum reached in our experiments ($17\,707.5\,\text{Gt}\,\text{yr}^{-1}$). The configurations for the different simulations are summarized in Table 1, and the data are publicly available at Mackie et al. (2020a). Anomalies presented later are the result of subtracting the value for a diagnostic in PIControl from the value for the same diagnostic in the experiment for the equivalent model time.

c. *Spatial distribution of the additional freshwater forcing*

The mean spatial distribution of the melt flux in PIControl is shown in Fig. 2a, alongside the anomaly showing the effect of the warming ocean surface on the meltwater distribution for the final 20 years of CO2 (Fig. 2b), and the anomalies showing how the additional melt flux is distributed for the final 20 years of FW and FWCO2 (Figs. 2c,d). Ocean surface properties in CO2 and PIControl differ, affecting iceberg trajectories and lifetimes, although both simulations are subject to the same total volume of iceberg mass. Similarly, the increased iceberg mass that is calved from the ice shelves is the same in FW as in FWCO2, but the additional iceberg melt is distributed differently because the ocean surface is warmer in FWCO2, and thus icebergs melt at higher latitudes.

TABLE 1. Summary of experiment and control simulation settings.

Model simulation	Other external forcings	Increasing mass loss
PIControl	Fixed preindustrial	No
FW	Fixed preindustrial	Yes
CO2	CO_2 increasing by 1% yr^{-1}	No
FWCO2	CO_2 increasing by 1% yr^{-1}	Yes

3. Results

a. *Sea ice effects*

Antarctic sea ice trends are spatially variable (Cavalieri and Parkinson 2008) and so we assess the sea ice response separately for the different ocean sectors in Fig. 3 (sectors defined following Yuan et al. 2017). The total melt flux entering each sector is shown in Fig. 4, and in this section we examine the sea ice response to this by looking at changes in sea ice area (SIA) (Fig. 5) and thickness (Fig. 6), relative to PIControl for the final 30 years of the simulations.

In CO2, sea ice area (Fig. 5a) and thickness (Fig. 6b) reduce as CO_2 increases and temperatures rise; however, this decrease is smaller than the increases in SIA and sea ice thickness attributable to increasing melt fluxes in FW (Figs. 5a, 6c). The combined effect of increasing melt fluxes and CO_2 in FWCO2 is a similar total SIA for the whole Southern Hemisphere to PIControl (Fig. 5a), rather than a net increase, because the warming ocean confines sea ice production to higher latitudes. This means that a greater proportion of the additional meltwater in FWCO2 enters the ocean where sea ice is unlikely to form, making the sensitivity of sea ice to the additional melt fluxes less pronounced in FWCO2 than in FW. Higher ocean temperatures in CO2 mean that where sea ice does form, it is thinner than in PIControl (Fig. 6b). In FWCO2, the additional melt fluxes mean that this lack of growth is partially offset, and in some places overcome, to result in thicker sea ice than in PIControl (Fig. 6d).

Regionally, the competing effects of the simultaneously increasing melt flux and CO_2 in the Ross Sea and Indian Ocean result in no net change to SIA in FWCO2, relative to PIControl (Figs. 5b,e). The Amundsen–Bellinghausen and Weddell Sea sectors receive the largest additional melt flux (Figs. 4c,d), and so melt-induced SIA-enhancing effects may be anticipated

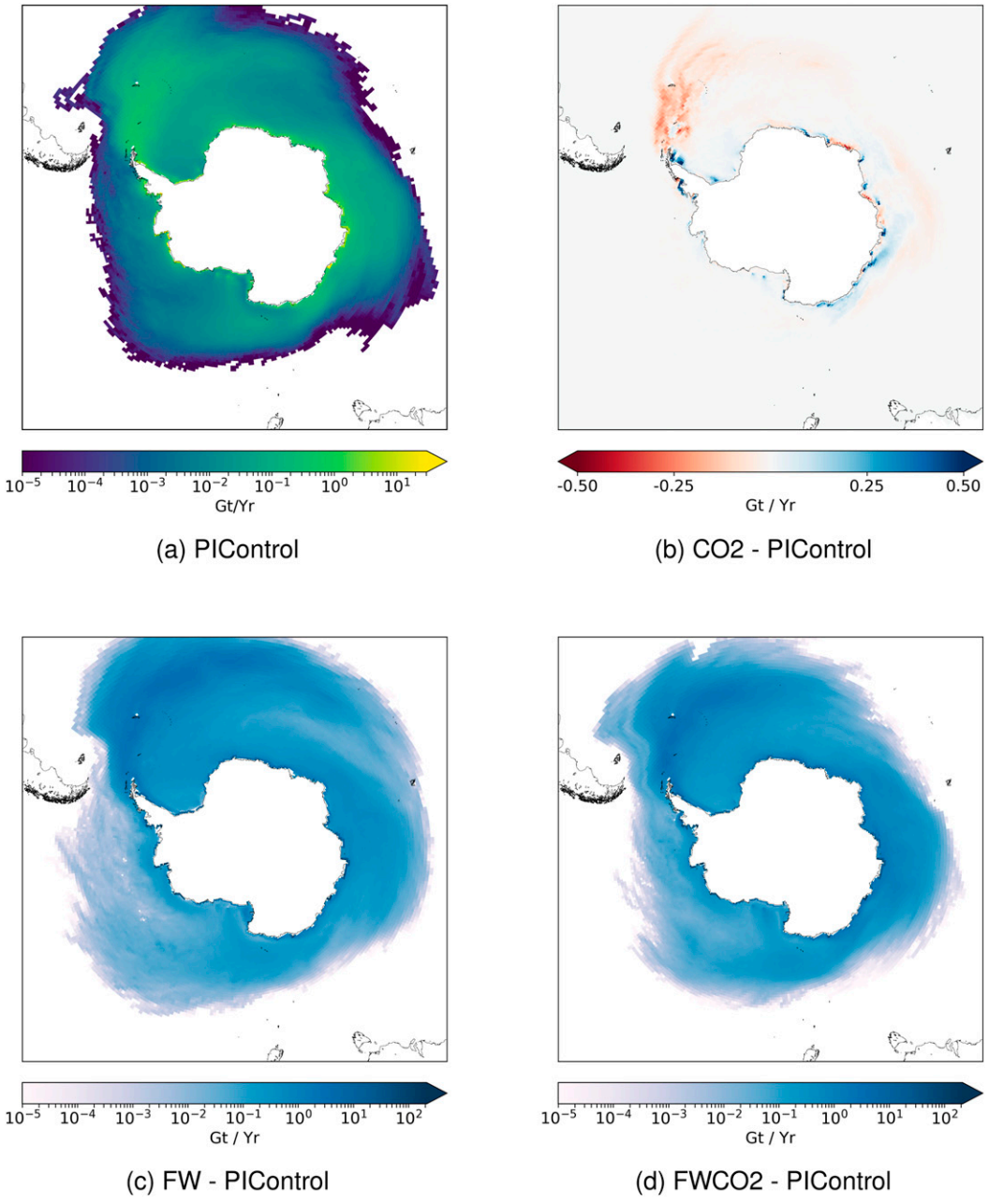

FIG. 2. (a) Mean spatial distribution of the total melt flux for PIControl. (b)–(d) The mean anomaly, with respect to PIControl, for the final 20 years of (b) CO2, (c) FW, and (d) FWCO2. Color scales for (a), (c), and (d) are logarithmic. Note the different color scale for the CO2 anomaly, where the total volume of meltwater is the same as for PIControl, and differences in the spatial distribution follow from the different ocean surface properties in a preindustrial environment and an environment of increasing CO_2.

to be stronger here than in the other sectors, and therefore more likely to override the effects of the CO_2. In both sectors, however, some ice shelf basal meltwater and icebergs are likely to be transported by the coastal current and the gyres (Fig. 3b). The Ross Gyre and coastal current carry some meltwater from the Amundsen–Bellinghausen Sea into the Ross Sea (freshwater transport across the boundary between these two sectors is plotted in Fig. S1 in the online supplemental material), and the Weddell Gyre carries icebergs, and some meltwater, generated in the Weddell Sea, northward to latitudes where sea ice is unlikely to form (Fig. 2). This

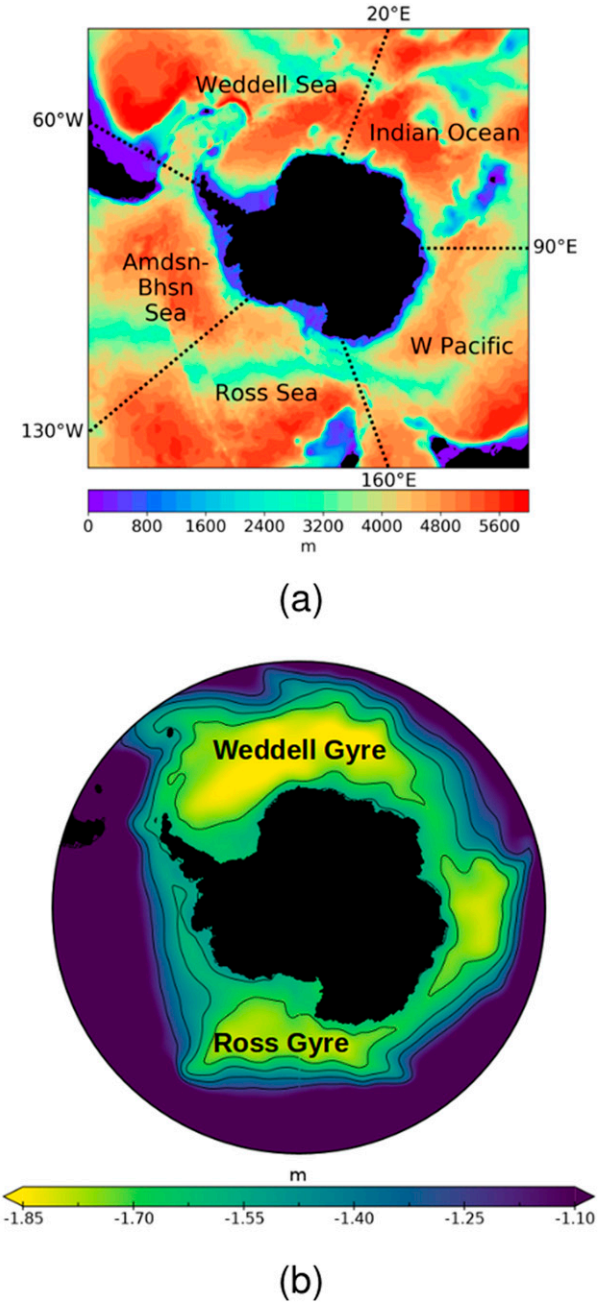

FIG. 3. (a) Bathymetry, with the ocean sectors (Ross Sea, Amundsen–Bellinghausen Sea, Weddell Sea, Indian Ocean, and western Pacific) used for discussion of sea ice effects overlaid. (b) Model sea surface height from PIControl, with closed contours indicating the centers for the Ross and Weddell Gyres referred to in the text. Note that the flow direction is clockwise for the gyres, and the Antarctic Coastal Current flows counterclockwise around the continent.

means that the increasing meltwater does not fully offset the SIA reduction driven by the CO_2, and SIA may in fact decrease slightly over the latter part of FWCO2 in these sectors (Fig. 5c,d). The decrease is small, and its persistence over a longer experiment would be required to determine whether effects from the increasing CO_2 locally dominate over those from the increasing melt fluxes.

The inclusion of increasing ice shelf and iceberg melt fluxes in FWCO2 serves to offset the decline in sea ice concentration in all sectors, cancelling it altogether (relative to preindustrial conditions) in every sector except the Amundsen–Bellinghausen Sea, where the additional freshwater weakens the decline, but does not altogether remove it (Fig. 5c). Data derived from satellite observations show sea ice around Antarctica to have been advancing in most areas in recent years, with the exception of the Amundsen–Bellinghausen Sea where the area has reduced, while climate models generally calculate it to be in decline everywhere (Cavalieri and Parkinson 2008; Stammerjohn et al. 2008; Turner et al. 2009). These results show that simulations where both CO_2 and meltwater fluxes increase simultaneously result in modeled sea ice area trends that agree more closely with satellite-derived datasets. It should be noted, however, that these are idealized simulations and realistic estimates for the increases in both CO_2 and meltwater depend on the future scenario assumed for greenhouse gas emissions.

The downward salt flux model output can be used as a proxy for sea ice production and used to identify areas of sea ice growth and decay. Before sea ice forms, all salt is in the ocean. When sea ice forms in the model, despite some brine rejection, both salt and freshwater are removed from the ocean and the salt is trapped in the sea ice (the salt amount is constant per unit volume of sea ice). Hence there is less salt than before in the ocean, and this constitutes an upward salt flux at the ocean surface. When sea ice melts, salt is returned to the ocean, constituting a downward salt flux at the ocean surface. The total salt content of the ocean is otherwise conserved and is unchanged by processes of adding freshwater or evaporation. Note that, since sea ice is relatively fresh, less salt is removed during sea ice production than is contained in the volume of ocean water that freezes, and the salinity of surface waters therefore increases with sea ice production.

Antarctic sea ice forms primarily in polynyas at the coast, although some also forms in the open ocean from frazil crystals at the surface, which in windless conditions, form a continuous flexible layer of thin ice, called nilas [as observed, for example, by Winsor and Björk (2000) and Smedsrud and Skogseth (2006)]. In windy conditions, wave action drives the formation of pancake ice from the frazil (Dai et al. 2004; Maksym 2012). The sea ice generally thickens through congelation (downward growth of ice crystals into the ocean), and through the accumulation of snow on the upper surface (Weeks

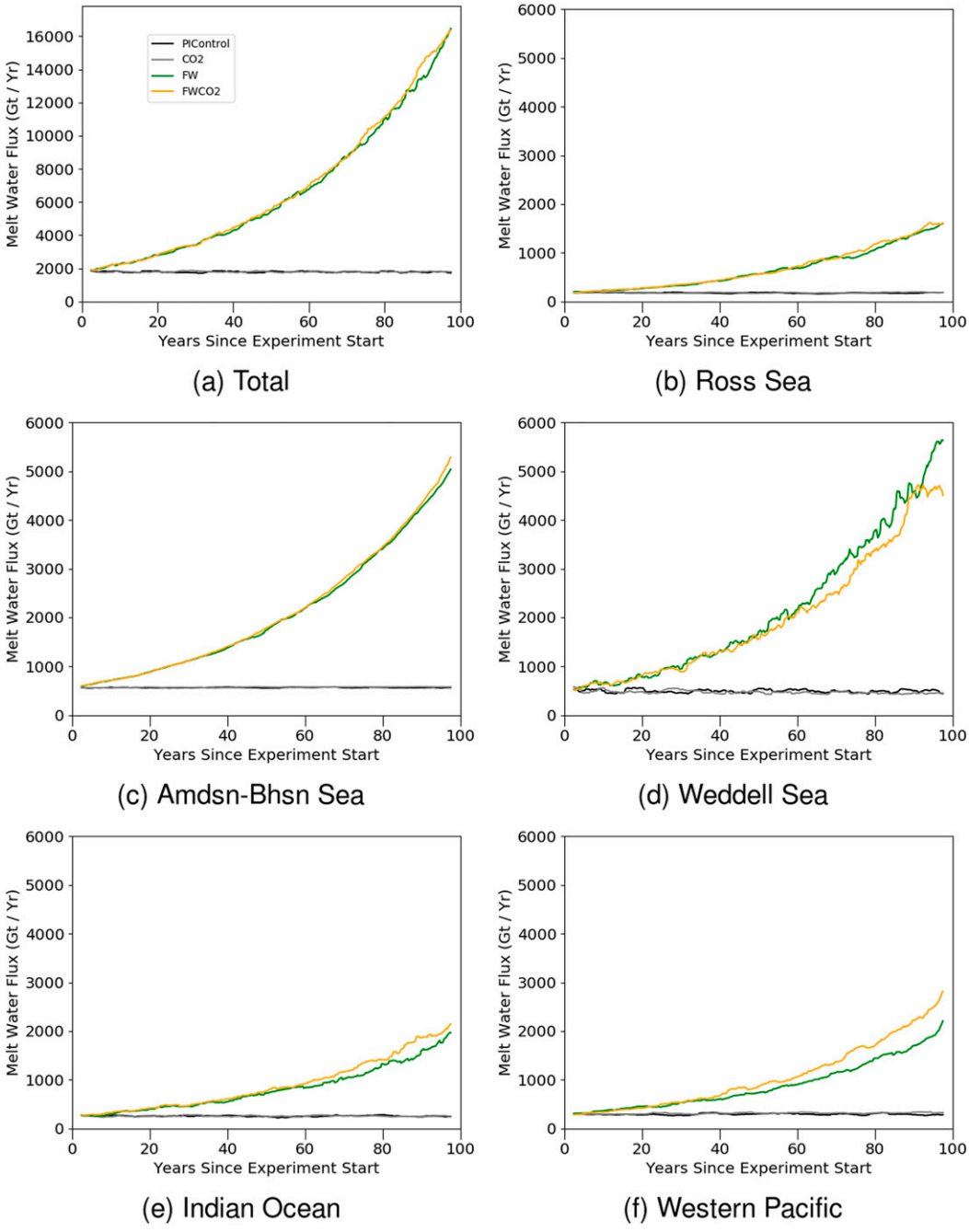

FIG. 4. Total melt flux in each simulation for the (a) whole Southern Hemisphere, (b) Ross Sea, (c) Amundsen–Bellinghausen Sea, (d) Weddell Sea, (e) Indian Ocean, and (f) western Pacific.

2010; Maksym 2012). Most Antarctic sea ice is transported equatorward and subsequently melts at the ice margins where the ocean is warmer (Weeks 2010; Maksym 2012).

Sea ice growth is greatest in June, July, and August in all experiments [the seasonal cycle for the simulations is plotted in the online supplemental material (Fig. S2)]. To assess changes to the spatial distribution of sea ice production, the mean anomaly in the downward salt flux for these months is shown in Fig. 7 for the final 30 years of all experiments, alongside the mean downward salt flux from PIControl for the same months. The positive (red) salt flux at the northern edge of the plotted data for PIControl (Fig. 7a) represents melting sea ice. In CO2, this flux is reduced since there is less sea ice here to melt

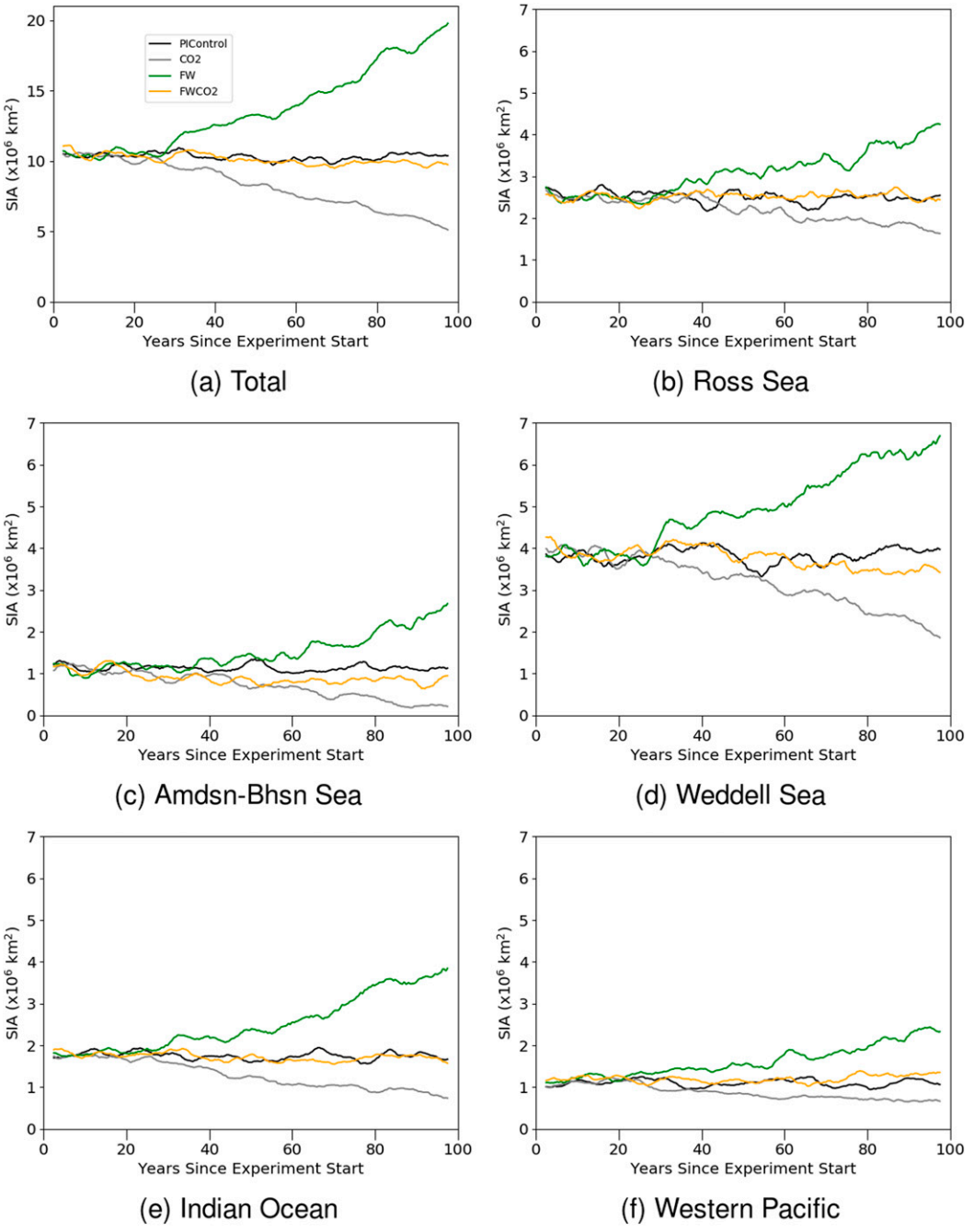

FIG. 5. Evolution of sea ice area (SIA) in each simulation for the (a) whole Southern Hemisphere, (b) Ross Sea, (c) Amundsen–Bellinghausen Sea, (d) Weddell Sea, (e) Indian Ocean, and (f) western Pacific (5-yr running mean).

in CO2 (Fig. 6b), creating the negative (blue) anomaly at the northern edge of Fig. 7b. Areas corresponding to a positive (red) anomaly in CO2 represent areas where sea ice production in PIControl is reduced, or has been replaced by sea ice melt. There is a slight increase in sea ice production in the Weddell and Ross Seas in CO2, and close to the coast around the western Indian Ocean, indicated by the blue anomaly in Fig. 7b.

The salt flux anomaly for CO2 (Fig. 7b) is spatially almost the inverse of that for FW (Fig. 7c). In FW, the northern melt edge is farther north than in PIControl because the sea ice has expanded (Fig. 6b). This creates the positive (red) anomaly at the northern edge in FW (since there is no sea ice here to melt in PIControl). The ring-like negative (blue) anomaly in FW indicates both reduced sea ice melt, and increased sea ice production

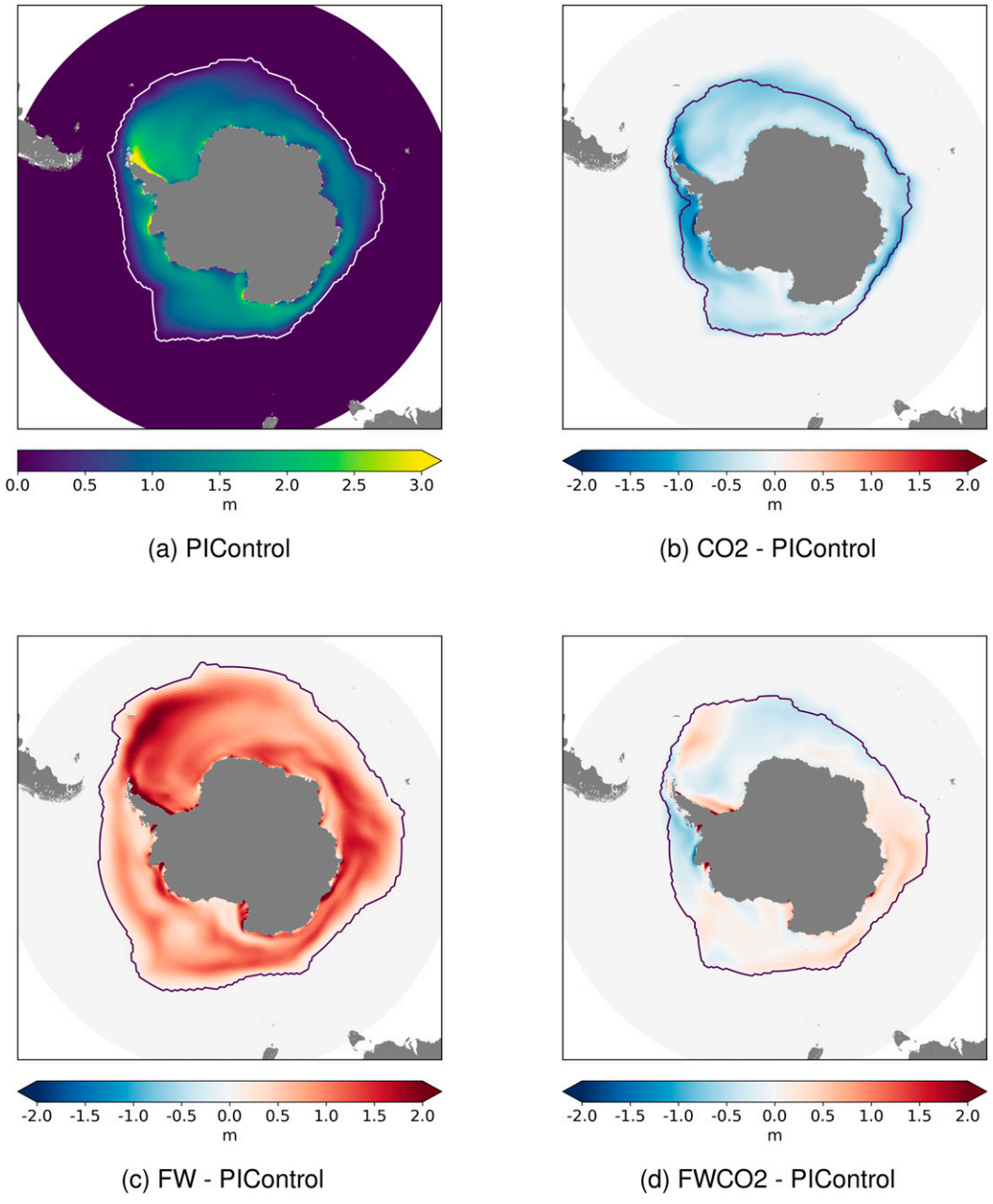

FIG. 6. (a) Mean September sea ice thickness (SIT) in PIControl. (b)–(d) SIT anomaly for the final 30 years of (b) CO2, (c) FW, and (d) FWCO2. The black contour [white in (a)] shows the mean September sea ice extent (the area beyond which the sea ice concentration in a grid cell does not exceed 15%) for (a) PIControl, (b) CO2, (c) FW, and (d) FWCO2.

(Fig. 7c), relative to PIControl. Southward of this blue ring, there is a positive anomaly in FW, which is particularly strong in the outer Weddell and Ross Seas, and in the western Indian Ocean. While sea ice production has increased strongly farther north in FW, it has decreased slightly here, relative to PIControl. In the western Pacific, where the continental shelf edge is close to the coast (Fig. 3a), the positive (red) anomaly at the coast in FW shows a reduction in sea ice production, while the negative (blue) anomaly beyond the coast, and beyond the continental shelf edge, shows increased sea ice production (Fig. 7c). This shift of at least some sea ice production in this area to beyond the continental shelf edge in FW is also seen, although more weakly, in FWCO2 (Fig. 7d). It is not seen in CO2, and must therefore be driven by the additional freshwater flux. In

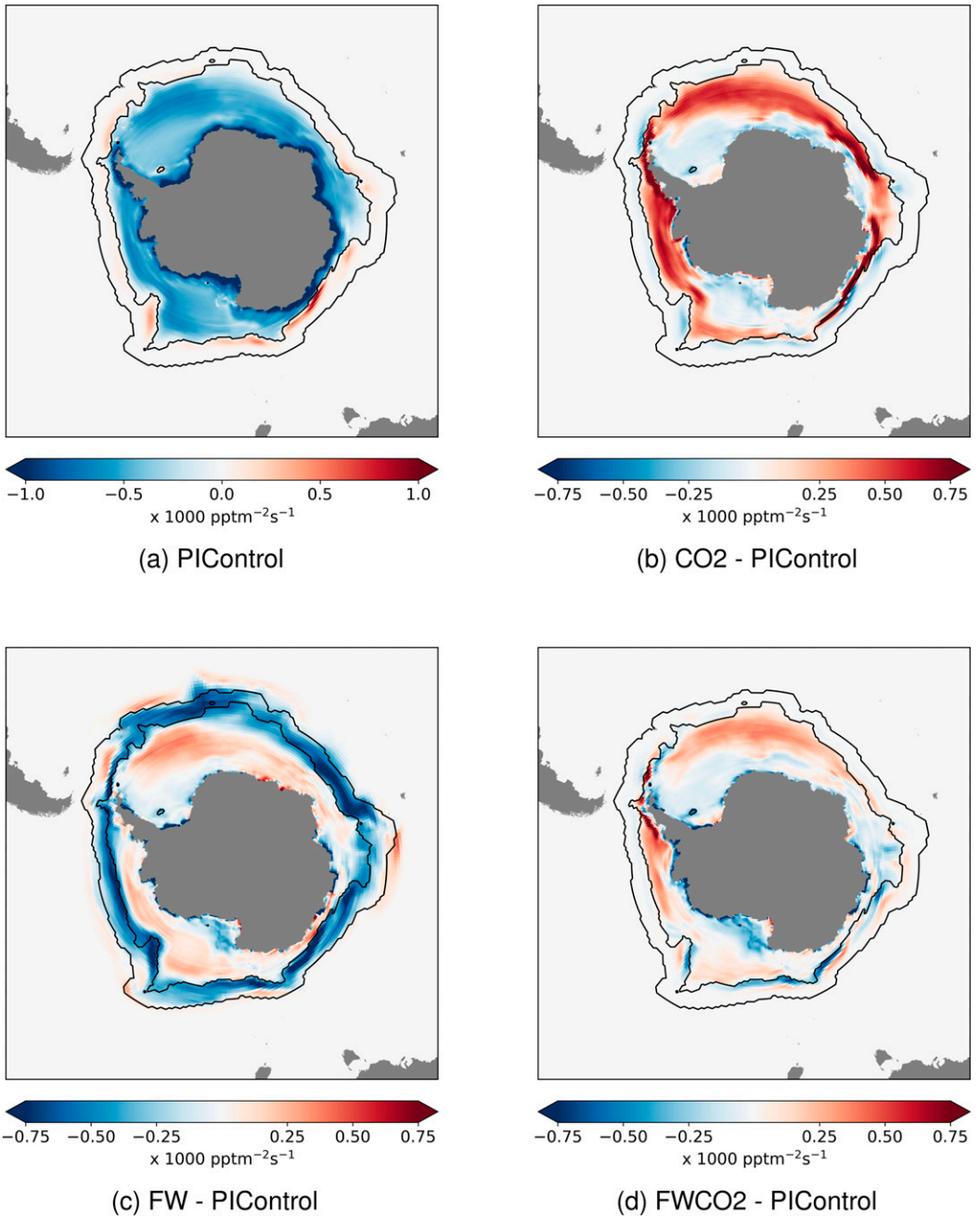

FIG. 7. (a) The mean downward salt flux for June, July, and August in PIControl. (b)–(d) Mean anomaly for June, July, and August for the final 30 years of (b) CO2, (c) FW, and (d) FWCO2. See text for an explanation of how this flux can be used as a proxy for sea ice production and decay. The contours on all panels show the extent of areas of sea ice production and melt in PIControl.

FWCO2, the competing effects of the increasing freshwater and CO_2 result in increased sea ice production over the continental shelf in the Ross and Weddell Seas, and also in the Indian Ocean, as shown by the negative (blue) anomaly in Fig. 7d. In the western Weddell Sea, there is an area of sea ice melt in PIControl, that is reduced FWCO2, and also in both FW and CO2, showing that this local effect follows from the increases in CO_2, and from the additional freshwater. The northern sea ice extent in FWCO2 (Fig. 7d) is similar to that in PIControl, showing that the increasing Antarctic melt flux has effectively balanced

the sea ice retreat induced by the CO_2, in agreement with Fig. 5.

b. *Effects on water mass formation*

As sea ice forms, brine is rejected, increasing the salinity of the ambient water. Ordinarily, in some places of rapid sea ice production over the continental shelf around Antarctica, this saline water is dense enough to sink to the depth of the shelf, and to spill over the shelf edge and spread through the deep ocean abyss as AABW (van Aken 2007; Nicholls et al. 2009). Another mechanism for AABW formation is prolonged deep convection in the open ocean, which is the primary mechanism by which AABW forms in most CMIP5 climate models but occurs rarely in reality (Heuzé et al. 2015; Cheon and Gordon 2019). Deep water convection does not occur in this configuration of HadGEM3-GC3.1 (Menary et al. 2018). Although the process of bottom-water formation has not been definitively determined, a strong salinity driven overturning at the Weddell Sea shelf break has been identified (Menary et al. 2018). The model physics and resolution are similar to ACCESS-OM 1.0, in which AABW is predominantly formed through convection over the continental shelf and subsequent transport of the dense sinking water over the shelf edge (Lago and England 2019). Changes to either the rate (Fig. 5), or the locations (Fig. 7), of Antarctic sea ice production in our model, may therefore result in changes to the mixed layer depth and to rates of AABW formation.

While seawater freezing into sea ice generally results in a deepening of the mixed layer as described above, melting ice shelves can also drive a deepening of the mixed layer if their melt rate is high enough (Merino et al. 2018; Mackie et al. 2020b). This is seen in some places along the coast in FW, where a high volume of buoyant ice shelf basal meltwater enters the ocean at depth and rises to the surface, resulting in a local overturning circulation (Fig. 8c). This overturning brings warmer waters to the surface, encouraging the formation and persistence of shore leads, which then promote sea ice production through enhanced frazil ice production, further contributing to persistence of the overturning through the associated brine rejection (Jourdain et al. 2017; Merino et al. 2018). Note that the freezing water in this case is relatively fresh and therefore associated with relatively weak brine rejection, and so while the surface water becomes saline enough to sustain the overturning (i.e., more saline than the rising freshwater), it is not dense enough to form AABW [density changes are shown in Fig. S3 in the online supplemental material and discussed further in Mackie et al. (2020b)]. In FWCO2 (Fig. 8d), where ice shelf basal melt rates are equal to those in FW, and enter the ocean with the same vertical and spatial distribution, this increased overturning at the coast is offset by the increasing CO_2, which reduces the temperature difference between the ocean surface and the air, and so shallows the mixed layer (Fig. 8b).

In other areas, where the depth or rate of ice shelf basal meltwater entering the ocean is insufficient to initialize a local overturning, the freshwater sits at the surface and forms a cap atop the water column, inhibiting further mixing and shallowing the mixed layer in FW. For example, the blue areas next to the coast in Fig. 8c in the eastern Weddell Sea, the western Indian Ocean, and parts of the Ross Sea, where the ice shelf melt rates and depths are relatively small [see Rignot et al. (2013), including supplementary materials]. In these areas, the surface freshening enhances the shallowing of the mixed layer driven by the increasing CO_2 to result in a strong shallowing in FWCO2, relative to PIControl (Fig. 8d).

To assess any impact on AABW, we use its northward transport as a proxy for formation rate. To compute the transport, we zonally integrate the meridional velocity at 30°S and then integrate this result vertically from the bottom of the ocean. We define the AABW transport as the first maximum of this function [following Heuzé et al. (2015) and Mackie et al. (2020b)] (Fig. 9a). The increased meltwater fluxes drive an increase in sea ice production, which may ordinarily be associated with increased AABW formation as described above. However, under preindustrial conditions in FW, the high volume of ice shelf basal meltwater causes a freshening of the whole water column, and consequently a reduction in AABW formation as water sinking to the shelf is less dense and therefore does not spill off and spread to fill the ocean abyss, (Mackie et al. 2020b). In the final 20 years of FW, AABW transport is 2.8 Sv weaker than in PIControl (Table 2). As CO_2 increases in CO2, the warming of the ocean makes the waters less dense, and so also drives a decrease in AABW formation. This results in AABW transport in the final 20 years of CO2 being 3.9 Sv weaker than in PIControl. The effect of increasing both ice shelf melt and CO_2 in FWCO2 is a slightly stronger decrease in AABW formation than in either FW or CO2, since in FWCO2 both the warming and the freshening drivers are present, and AABW transport for the final 20 years of FWCO2 is 4.6 Sv weaker than in PIControl. The changes in density that drive these changes in AABW transport are very small (of order 0.01 $kg\,m^{-3}$), and are plotted in the online supplemental material (Fig. S3). A Student's *t* test for related samples, comparing AABW for the final 20 years of each of the experiments with that in PIControl for the

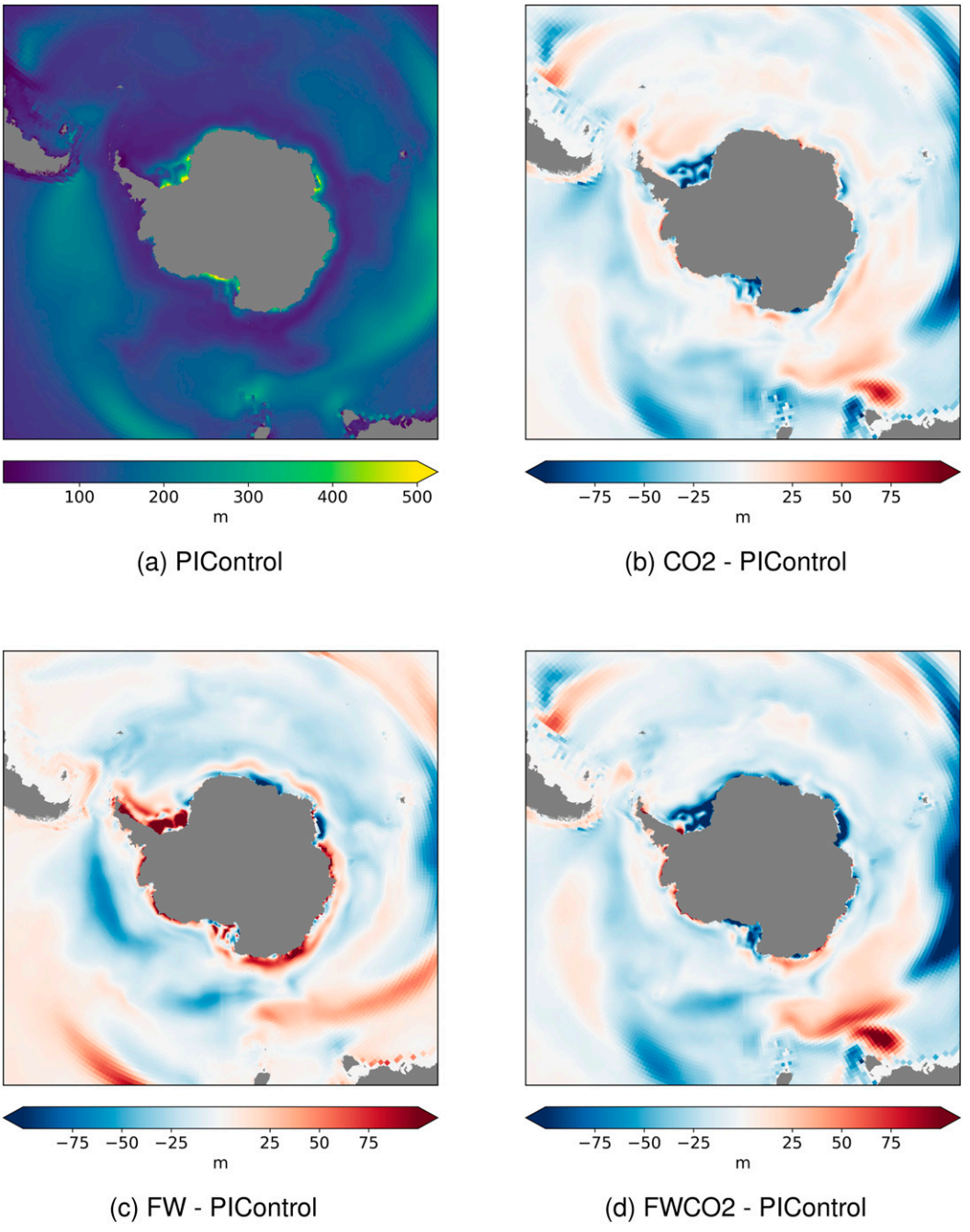

FIG. 8. (a) The mean mixed layer depth for June, July, and August in PIControl. (b)–(d) Mean anomaly for June, July, and August for the final 30 years of (b) CO2, (c) FW, and (d) FWCO2. Mixed layer depth is defined as the depth at which the potential density of seawater differs from that at 10 m depth by more than 0.01 kgm^{-3}.

same period, shows all these changes to be statistically significant at a greater than 99% confidence level (Table 2). Although the mechanism for the decline in AABW formation in FWCO2 is partly a freshening of the whole water column, rather than increased stratification as found by Lago and England (2019), these findings do support the suggestion raised in that work that the decline in AABW formation projected under global warming scenarios may be weaker than in reality if the projections do not account for increasing melt fluxes from Antarctica.

Changes in AABW export from the Antarctic have been linked to changes in the Atlantic meridional overturning circulation (AMOC) (Weaver et al. 2003;

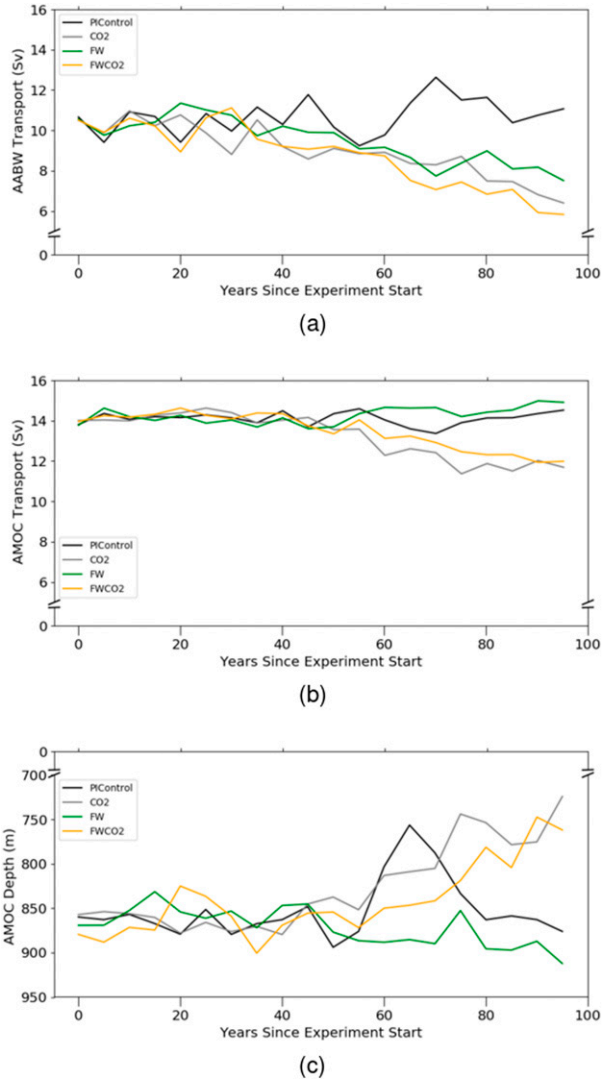

FIG. 9. (a) The zonal mean maximum AABW transport at 30°S. (b) AMOC strength at 30°S. (c) AMOC depth at 30°S. The 5-yr running mean is shown in all panels. See text for a description of calculations for the AMOC strength and depth.

Swingedouw et al. 2009), which is important to Northern Hemisphere climate (Buckley and Marshall 2016; Sévellec and Fedorov 2016). A reduction in AABW export can allow the AMOC to reach farther south in the Atlantic at greater depth (Swingedouw et al. 2009). We therefore examine both the strength (Fig. 9b) and depth (Fig. 9c) of the AMOC at 30°S. We integrate the meridional velocity at 30°S through the Atlantic basin from coast to coast. We then integrate this result over depth, from the bottom of the ocean to the surface. We define the AMOC strength at 30°S as the maximum of this integrated transport in the southward direction (following Heuzé et al. 2015), and the AMOC depth as the depth at which this maximum occurs. We use a Student's *t* test to compare the AMOC strength and depth for final 20 years of the experiments with that in PIControl for the same period, and assess the significance of any change (Table 2). In PIControl, the mean AMOC strength is 14.22 Sv. In FW, there is a small strengthening (0.4 Sv), significant at the 95% confidence level, and the AMOC becomes slightly deeper (by 32 m) at 30°S in response to the reduced AABW transport, (Fig. 9c). In CO2, the AMOC weakens by 2.5 Sv and becomes around 108 m shallower (relative to PIControl), following the CO_2-induced warming (see also Rahmstorf et al. 2015) (Figs. 9b,c). The CO_2-induced weakening and shallowing of the AMOC in CO2 are greater than the changes driven by the reduced AABW transport following the increased ice shelf melt in FW, and are statistically more significant with a confidence level exceeding 99%. In FWCO2, the CO_2-induced weakening and shallowing of the AMOC may be slightly offset by the effects of the reduced AABW transport in the second half of the simulations [when the reduction in AABW transport is greater in FWCO2 than in CO2 (Fig. 9a)], although the variability of the AMOC in all the simulations means a longer time series would be required to conclude this definitively (Fig. 9b). This suggests that, while climate projections that neglect increasing Antarctic melt fluxes may underestimate the future decline in AABW, they may slightly overestimate the decline in the AMOC at southern latitudes.

c. *Surface ocean effects*

An increasing volume of meltwater entering the Southern Ocean causes surface waters to cool and freshen, as buoyant freshwater sits at the surface and

TABLE 2. Difference in the mean AABW and AMOC transport and AMOC depth between each experiment and PIControl for the final 20 years of the simulations. The significance of any change is given by the *p* value (following from calculation of the *t* score for related samples). A *p* value of less than 0.05 indicates significance at the 95% confidence level.

Simulation	Δ AABW transport (Sv)	*p* value	Δ AMOC transport (Sv)	*p* value	Δ AMOC depth (m)	*p* value
PIControl–CO2	3.914	2.4×10^{-45}	2.504	6.0×10^{-31}	−107.589	8.9×10^{-64}
PIControl–FW	2.796	8.3×10^{-30}	−0.427	0.014	32.021	1.0×10^{-15}
PIControl–FWCO2	4.561	7.3×10^{-52}	2.145	9.5×10^{-26}	−91.720	6.3×10^{-56}

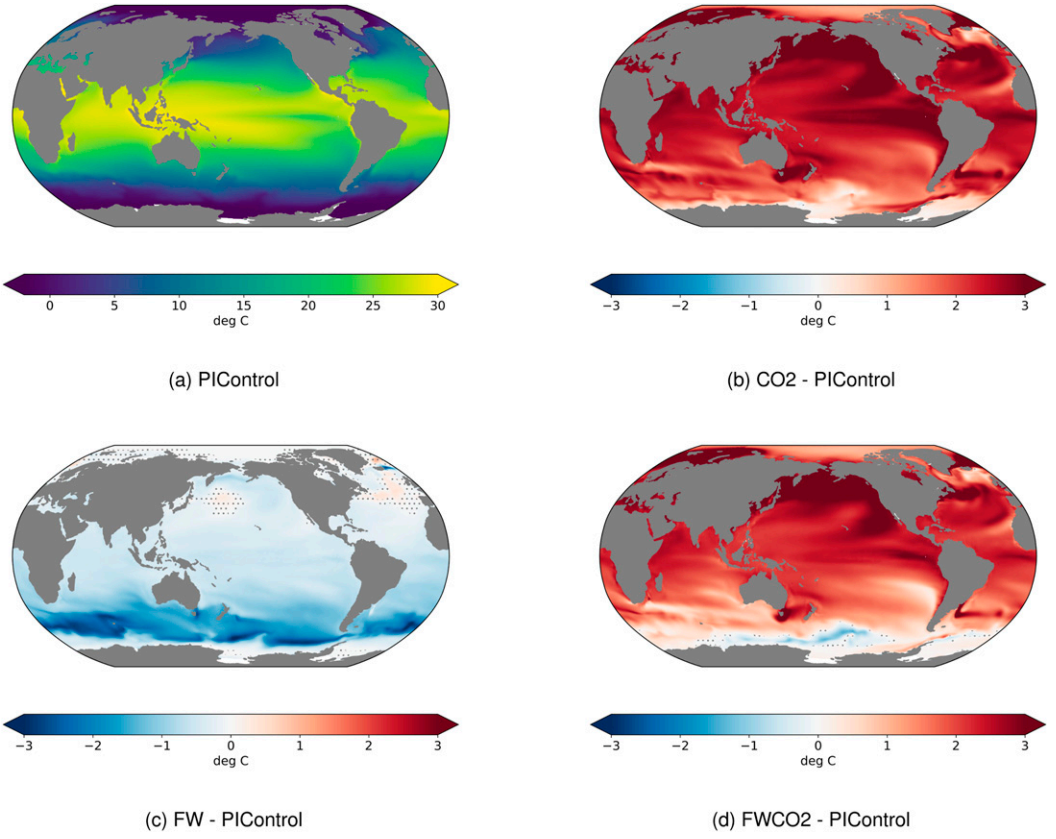

FIG. 10. (a) Mean sea surface temperature (SST) in PIControl. (b)–(d) SST anomaly, averaged over the final 30 years of (b) CO2, (c) FW, and (d) FWCO2. Stippling marks anomalies not significant at the 95% confidence level (using a Student's *t* test for related samples).

drives stratification of the water column, and these effects may extend into the Northern Hemisphere (Richardson et al. 2005; Pauling et al. 2017; Bronselaer et al. 2018; Mackie et al. 2020b). Globally increasing CO_2 causes the ocean to warm everywhere, and we consider whether the effect of a simultaneous increase in meltwater could partially offset this (Fig. 10). Similar effects were found for all seasons (not shown). The strong warming that occurs everywhere in CO2, as a result of the increasing CO_2, is reduced slightly in the tropical Pacific, the North Atlantic, and in the northwestern Indian Ocean as a result of the increased Antarctic mass loss in FWCO2, but the warming in these areas is not reversed. A stronger reduction in the surface warming occurs in the southern Indian, Atlantic, and Pacific Oceans, closer to the source of the melt perturbation. Closer to Antarctica, in the outer Ross Sea and in the southwestern Pacific, the warming in CO2 is replaced by a cooling in FWCO2 (relative to PIControl), while waters next to the coast are likely to be at, or close to, their freezing temperature in all simulations, and therefore do not cool further. The increasing melt volume in FWCO2 does not significantly alter the changes in surface salinity seen in CO2 (which are attributable to increasing CO_2), except at very high southern latitudes, where there is increased freshening [shown in the online supplementary material (Fig. S4)].

Under preindustrial conditions in FW, surface cooling and freshening from the increased ice shelf melt flux causes an increase in near surface ocean density at high southern latitudes that is mainly temperature driven [see Mackie et al. (2020b) for more details of this effect]. This reduces the meridional density gradient across the Southern Ocean, driving a reduction in the Antarctic Circumpolar Current (ACC) volume transport, potentially altering the flow of heat to the high-latitude ocean (Russell et al. 2006; Mackie et al. 2020b). The response of the ACC to the increasing melt in FWCO2 is similar to that in FW for the first 50 years, however, as both CO_2 and the melt increase further over the final 50 years, the ACC transport in FWCO2 becomes similar to that in CO2, where only CO_2 is increasing. This is because the CO_2-induced warming of the surface ocean in FWCO2 greatly reduces the near-surface density everywhere (a plot of the

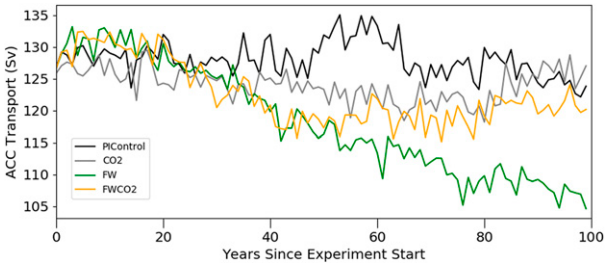

FIG. 11. Annual mean of the Antarctic Circumpolar Current (ACC) transport, calculated as integrated mass transport across the Drake Passage.

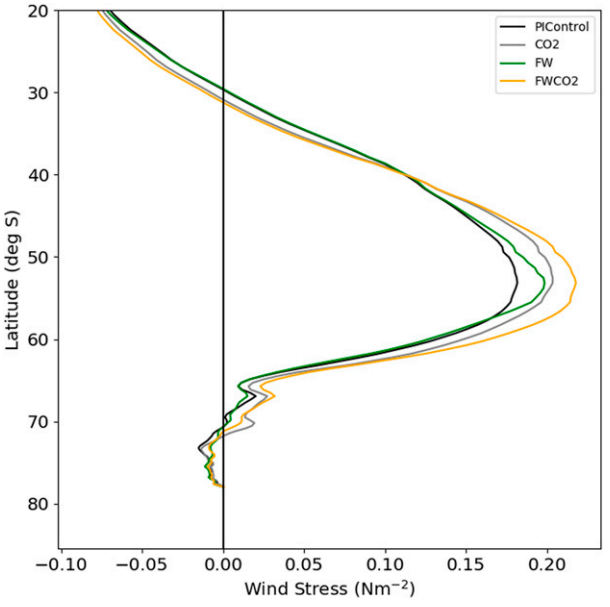

FIG. 12. Zonal mean westerly wind stress for August to October, averaged over the final 30 years of the experiments.

density anomalies is included in Fig. S3 in the online supplemental material). The additional melt in FWCO2 drives a surface cooling at high latitudes, but after 50 years, this is weaker than in FW (Fig. 10), and the density changes resulting from the additional melt in FWCO2 are therefore not strong enough to alter the meridional density gradient and impact the ACC in the second half of the simulation (Fig. 11).

d. Effects on wind stress

The westerly wind belt around Antarctica is driven in part by the meridional gradient in the vertical exchange of heat between the ocean and atmosphere (Kidston et al. 2011). Sea ice insulates the ocean surface and so inhibits this flux at high latitudes, suggesting a link between sea ice extent and the strength and position of the winds that has been investigated in several studies (Menéndez et al. 1999; Kidston et al. 2011; Bader et al. 2013; Grise and Polvani 2016; Bracegirdle et al. 2018). Surface cooling also reduces the ocean to atmosphere heat flux, strengthening the westerly winds (Mackie et al. 2020b). Increasing meltwater offsets the CO_2-induced decline in sea ice extent (Fig. 6) and cools the ocean surface (Fig. 10), and so we consider whether the strengthening of the winds that is generally associated with increasing CO_2 (Swart and Fyfe 2012) may be affected by the increased meltwater.

The sensitivity of the surface wind stress to sea ice concentration is greatest in August September and October (Kidston et al. 2011) at maximum sea ice extent. The simulated zonal mean westerly wind stress, at this time, is shown in Fig. 12. Both the increased CO_2 (CO2) and the increased melt fluxes (FW) drive an increase in wind stress at the surface, which we interpret as an increase in jet strength. The greatest strengthening of the wind stress occurs when both forcings are applied together in FWCO2 (Fig. 12). To assess whether there was a significant change by the end of the experiments, the mean strength and position for the peak wind stress over the final 20 years of each experiment were compared to those for PIControl, averaged over the same period, using a *t* test for related samples to calculate the significance. We calculated the strength and position of the peak wind stress from a quadratic curve fitted to the three model grid points surrounding the maximum wind stress (Fig. 12) for the comparison (Table 3). There is no significant change to the latitude for the maximum wind stress in any of the experiments. Increasing the meltwater fluxes in FW results in the peak wind stress increasing by 0.019 N m^{-2} at the 95% confidence level, and the increasing CO_2 in CO2 drives an increase of 0.033 N m^{-2} at a confidence level greater than 99%. The greatest increase in strength, 0.043 N m^{-2}, is in FWCO2, when both drivers are present. Including increasing Antarctic meltwater fluxes may therefore partially address the bias common to many climate models, whereby the simulated westerly winds are too weak when compared to reanalysis data (Bracegirdle et al. 2013).

4. Summary

Almost all the projections in CMIP5 and CMIP6 suggest a strong decline in Antarctic sea ice under future climate warming scenarios, but none of these models include an increase in the ice shelf melt fluxes from Antarctica. Our results show that these increasing melt fluxes may enhance sea ice growth and partially offset a CO_2-induced decline in Antarctic sea ice area and thickness.

We have shown that including increasing ice sheet and iceberg melt fluxes in climate models could reduce some

TABLE 3. Difference between the mean peak westerly wind stress over the Southern Ocean for each experiment and PIControl for the final 20 years of the simulations. The peak strength is the strength at the peak location in Fig. 12, determined as described in the text. The significance of any change is given by the p value (following from calculation of the t score for related samples). A p value of less than 0.05 indicates significance at the 95% confidence level.

Simulation	Δ Latitude (°)	p value	Δ Strength (N m^{-2})	p value
CO2	−0.687	0.646	**0.033**	**2.49×10^{-7}**
FW	−1.045	0.379	**0.019**	**0.011**
FWCO2	−1.107	0.428	**0.043**	**2.59×10^{-8}**

model biases, and our results demonstrate the importance of considering the effect of combined forcings when determining sensitivities for future climate projections. Some responses to increasing ice shelf and iceberg melt fluxes in the Southern Ocean may be balanced by increasing levels of CO_2. For example, the local overturning of Antarctic coastal waters, initiated by large increases in ice shelf basal melt entering the ocean at depth, is inhibited if CO_2 increases simultaneously with the melt rate. The separate forcings (increasing CO_2 and increasing Antarctic mass loss) combine to result in a greater reduction in AABW formation and a greater strengthening of westerly wind stress than is seen when either forcing is applied in isolation. In other areas, the warming effect of the CO_2 is partially countered by the increasing melt flux. For example, slightly more moderate surface temperature increases are seen in the Southern Ocean and there is no clear net reduction in sea ice area. The reduction in the ACC that follows from density changes induced by increased ice shelf basal melt is not seen when CO_2 increases simultaneously, because of the more severe and widespread density changes associated with the CO_2 increase.

These are idealized experiments and the increase implemented for the Antarctic melt rate was spatially uniform, whereas in reality it is likely that melt rates will accelerate more for some ice shelves than for others, which may alter the sensitivities found here. Similarly, the increase in CO_2 is also idealized and the impact of increasing CO_2, and the sensitivity of this to increasing melt rates, will depend on future emission rates for greenhouse gases.

Increasing Antarctic melt fluxes, which are more likely as the ocean warms and ice shelves become negatively mass balanced, have an impact on global climate. Future climate projections that neglect the increasing melt rates are likely to overestimate both Antarctic sea ice decline and some ocean surface warming in the Southern Hemisphere. Similarly, both the decrease in AABW formation, and the strengthening of the westerly winds around Antarctica may be underestimated in current climate projections. The effects of increasing CO_2 and increasing melt fluxes are interactive and their combined effect is not a linear sum of the effects that they drive individually (i.e., when implemented separately). It is therefore important that increasing Antarctic melt fluxes be realistically represented in climate models, perhaps through an embedded dynamic ice sheet model, in order that the impact of future warming on sea ice, ocean, and climate be reliably projected.

Acknowledgments. This project was funded by the New Zealand Deep South National Science Challenge, MBIE contract C01 × 142. Data for PIControl and CO2 were calculated by the Hadley Centre, U.K. Met Office for submission to the CMIP6 experiment. The project is grateful for support from Professor Bitz at University of Washington. We acknowledge use of the Monsoon2 system, and the High Capacity Central File Storage Service at University of Otago, New Zealand. Model data analyzed in this work are publicly available at Mackie et al. (2020a).

REFERENCES

Andreas, E. L, and B. Murphy, 1986: Bulk transfer coefficients for heat and momentum over leads and polynyas. *J. Phys. Oceanogr.*, **16**, 1875–1883, https://doi.org/10.1175/1520-0485(1986)016<1875:BTCFHA>2.0.CO;2.

Bader, J., M. Flügge, N. G. Kvamstø, M. D. S. Mesquita, and A. Voigt, 2013: Atmospheric winter response to a projected future Antarctic sea-ice reduction: A dynamical analysis. *Climate Dyn.*, **40**, 2707–2718, https://doi.org/10.1007/s00382-012-1507-9.

Bigg, G. R., M. R. Wadley, D. P. Stevens, and J. A. Johnson, 1997: Modelling the dynamics and thermodynamics of icebergs. *Cold Reg. Sci. Technol.*, **26**, 113–135, https://doi.org/10.1016/S0165-232X(97)00012-8.

Bintanja, R., G. J. van Oldenborgh, S. S. Drijfhout, B. Wouters, and C. A. Katsman, 2013: Important role for ocean warming and increased ice-shelf melt in Antarctic sea-ice expansion. *Nat. Geosci.*, **6**, 376–379, https://doi.org/10.1038/ngeo1767.

——, ——, and C. Katsman, 2015: The effect of increased fresh water from Antarctic ice shelves on future trends in Antarctic sea ice. *Ann. Glaciol.*, **56**, 120–126, https://doi.org/10.3189/2015AoG69A001.

Bracegirdle, T. J., E. Shuckburgh, J.-B. Sallee, Z. Wang, A. J. S. Meijers, N. Bruneau, T. Phillips, and L. J. Wilcox, 2013: Assessment of surface winds over the Atlantic, Indian, and Pacific Ocean sectors of the Southern Ocean in CMIP5

models: Historical bias, forcing response, and state dependence. *J. Geophys. Res. Atmos.*, **118**, 547–562, https://doi.org/10.1002/JGRD.50153.

——, P. Hyder, and C. R. Holmes, 2018: CMIP5 diversity in southern westerly jet projections related to historical sea ice area: Strong link to strengthening and weak link to shift. *J. Climate*, **31**, 195–211, https://doi.org/10.1175/JCLI-D-17-0320.1.

Bromwich, D. H., B. Chen, K. M. Hines, and R. I. Cullather, 1998: Global atmospheric responses to Antarctic forcing. *Ann. Glaciol.*, **27**, 521–527, https://doi.org/10.3189/1998AoG27-1-521-527.

Bronselaer, B., M. Winton, S. M. Griffies, W. J. Hurlin, K. B. Rodgers, O. V. Sergienko, R. J. Stouffer, and J. L. Russell, 2018: Change in future climate due to Antarctic meltwater. *Nature*, **564**, 53–58, https://doi.org/10.1038/s41586-018-0712-z.

Buckley, M. W., and J. Marshall, 2016: Observations, inferences, and mechanisms of the Atlantic meridional overturning circulation: A review. *Rev. Geophys.*, **54**, 5–63, https://doi.org/10.1002/2015RG000493.

Cavalieri, D. J., and C. L. Parkinson, 2008: Antarctic sea ice variability and trends, 1979–2006. *J. Geophys. Res.*, **113**, C07004, https://doi.org/10.1029/2007JC004564.

Cheon, W. G., and A. L. Gordon, 2019: Open-ocean polynyas and deep convection in the Southern Ocean. *Sci. Rep.*, **9**, 6935, https://doi.org/10.1038/s41598-019-43466-2.

Dai, M., H. H. Shen, M. A. Hopkins, and S. F. Ackley, 2004: Wave rafting and the equilibrium pancake ice cover thickness. *J. Geophys. Res.*, **109**, C07023, https://doi.org/10.1029/2003JC002192.

DeConto, R. M., and D. Pollard, 2016: Contribution of Antarctica to past and future sea-level rise. *Nature*, **531**, 591–597, https://doi.org/10.1038/nature17145.

Grise, K. M., and L. M. Polvani, 2016: Is climate sensitivity related to dynamical sensitivity? *J. Geophys. Res. Atmos.*, **121**, 5159–5176, https://doi.org/10.1002/2015JD024687.

Heuzé, C., K. J. Heywood, D. P. Stevens, and J. K. Ridley, 2015: Changes in global ocean bottom properties and volume transports in CMIP5 models under climate change scenarios. *J. Climate*, **28**, 2917–2944, https://doi.org/10.1175/JCLI-D-14-00381.1.

Hoskins, B. J., and K. I. Hodges, 2005: A new perspective on southern hemisphere storm tracks. *J. Climate*, **18**, 4108–4129, https://doi.org/10.1175/JCLI3570.1.

Jourdain, N. C., P. Mathiot, N. Merino, G. Durand, J. Le Sommer, P. Spence, P. Dutrieux, and G. Madec, 2017: Ocean circulation and sea-ice thinning induced by melting ice shelves in the Amundsen Sea. *J. Geophys. Res. Oceans*, **122**, 2550–2573, https://doi.org/10.1002/2016JC012509.

Kidston, J., A. S. Taschetto, D. W. J. Thompson, and M. H. England, 2011: The influence of southern hemisphere sea-ice extent on the latitude of the mid-latitude jet stream. *Geophys. Res. Lett.*, **38**, L15804, https://doi.org/10.1029/2011GL048056.

Kuhlbrodt, T., and Coauthors, 2018: The low-resolution version of HadGEM3 GC3.1: Development and evaluation for global climate. *J. Adv. Model. Earth Syst.*, **10**, 2865–2888, https://doi.org/10.1029/2018MS001370.

Lago, V., and M. H. England, 2019: Projected slowdown of Antarctic bottom water formation in response to amplified meltwater contributions. *J. Climate*, **32**, 6319–6335, https://doi.org/10.1175/JCLI-D-18-0622.1.

Le Quéré, C., and Coauthors, 2007: Saturation of the Southern Ocean CO_2 sink due to recent climate change. *Science*, **316**, 1735–1738, https://doi.org/10.1126/science.1136188.

Liston, G. E., and J.-G. Winther, 2005: Antarctic surface and subsurface snow and ice melt fluxes. *J. Climate*, **18**, 1469–1481, https://doi.org/10.1175/JCLI3344.1.

Mackie, S., I. J. Smith, J. K. Ridley, D. P. Stevens, and P. J. Langhorne, 2020a: Climate model response to increasing Antarctic iceberg and ice shelf melt. PANGAEA, https://doi.org/10.1594/PANGAEA.911392.

——, ——, ——, ——, and ——, 2020b: Climate response to increasing Antarctic iceberg and ice shelf melt. *J. Climate*, **33**, 8917–8938, https://doi.org/10.1175/JCLI-D-19-0881.1.

Maksym, T., 2012: Antarctic sea ice—A polar opposite? *Oceanography*, **25**, 140–151, https://doi.org/10.5670/oceanog.2012.88.

Marsh, R., and Coauthors, 2015: NEMO-ICB (v1.0): Interactive icebergs in the NEMO ocean model globally configured at eddy-permitting resolution. *Geosci. Model Dev.*, **8**, 1547–1562, https://doi.org/10.5194/gmd-8-1547-2015.

Marsland, S. J., J. A. Church, N. L. Bindoff, and G. D. Williams, 2007: Antarctic coastal polynya response to climate change. *J. Geophys. Res.*, **112**, C07009, https://doi.org/10.1029/2005JC003291.

Martín-Español, A., and Coauthors, 2016: Spatial and temporal Antarctic ice sheet mass trends, glacio-isostatic adjustment, and surface processes from a joint inversion of satellite altimeter, gravity, and GPS data. *J. Geophys. Res. Earth Surf.*, **121**, 182–200, https://doi.org/10.1002/2015JF003550.

Mathiot, P., A. Jenkins, C. Harris, and G. Madec, 2017: Explicit representation and parametrised impacts of under ice shelf seas in the z^* coordinate ocean model NEMO 3.6. *Geosci. Model Dev.*, **10**, 2849–2874, https://doi.org/10.5194/gmd-10-2849-2017.

Menary, M. B., and Coauthors, 2018: Preindustrial control simulations with HadGEM3-GC3.1 for CMIP6. *J. Adv. Model. Earth Syst.*, **10**, 3049–3075, https://doi.org/10.1029/2018MS001495.

Menéndez, C. G., V. Serafini, and H. Le Treut, 1999: The effect of sea-ice on the transient atmospheric eddies of the southern hemisphere. *Climate Dyn.*, **15**, 659–671, https://doi.org/10.1007/s003820050308.

Merino, N., N. C. Jourdain, J. L. Sommer, H. Goosse, P. Mathiot, and G. Durand, 2018: Impact of increasing Antarctic glacial freshwater release on regional sea-ice cover in the Southern Ocean. *Ocean Modell.*, **121**, 76–89, https://doi.org/10.1016/j.ocemod.2017.11.009.

Nicholls, K. W., S. Østerhus, K. Makinson, T. Gammelsrød, and E. Fahrbach, 2009: Ice-ocean processes over the continental shelf of the southern Weddell Sea, Antarctica: A review. *Rev. Geophys.*, **47**, RG3003, https://doi.org/10.1029/2007RG000250.

Pauling, A. G., C. M. Bitz, I. J. Smith, and P. J. Langhorne, 2016: The response of the Southern Ocean and Antarctic sea ice to freshwater from ice shelves in an Earth system model. *J. Climate*, **29**, 1655–1672, https://doi.org/10.1175/JCLI-D-15-0501.1.

——, I. J. Smith, P. J. Langhorne, and C. M. Bitz, 2017: Time-dependent freshwater input from ice shelves: Impacts on Antarctic sea ice and the Southern Ocean in an Earth system model. *Geophys. Res. Lett.*, **44**, 10 454–10 461, https://doi.org/10.1002/2017GL075017.

Rahmstorf, S., J. E. Box, G. Feulner, M. E. Mann, A. Robinson, S. Rutherford, and E. J. Schaffernicht, 2015: Exceptional twentieth-century slowdown in Atlantic Ocean overturning circulation. *Nat. Climate Change*, **5**, 475–480, https://doi.org/10.1038/nclimate2554.

Richardson, G., M. R. Wadley, K. J. Heywood, D. P. Stevens, and H. T. Banks, 2005: Short-term climate response to a freshwater

pulse in the Southern Ocean. *Geophys. Res. Lett.*, **32**, L03702, https://doi.org/10.1029/2004GL021586.

Ridley, J. K., E. W. Blockley, A. B. Keen, J. G. L. Rae, A. E. West, and D. Schroeder, 2018: The sea ice model component of HadGEM3-GC3.1. *Geosci. Model Dev.*, **11**, 713–723, https://doi.org/10.5194/gmd-11-713-2018.

Rignot, E., J. L. Bamber, M. R. van den Broeke, C. Davis, Y. Li, W. J. van de Berg, and E. van Meijgaard, 2008: Recent Antarctic ice mass loss from radar interferometry and regional climate modelling. *Nat. Geosci.*, **1**, 106–110, https://doi.org/10.1038/ngeo102.

——, S. Jacobs, J. Mouginot, and B. Scheuchl, 2013: Ice-shelf melting around Antarctica. *Science*, **341**, 266–270, https://doi.org/10.1126/science.1235798.

Rind, R., R. Healy, C. Parkinson, and D. Martinson, 1995: The role of sea ice in $2\times CO_2$ climate model sensitivity. Part I: The total influence of sea ice thickness and extent. *J. Climate*, **8**, 449–463, https://doi.org/10.1175/1520-0442(1995)008<0449:TROSII>2.0.CO;2.

Russell, J. L., R. J. Stouffer, and K. W. Dixon, 2006: Intercomparison of the Southern Ocean circulations in IPCC coupled model control simulations. *J. Climate*, **19**, 4560–4575, https://doi.org/10.1175/JCLI3869.1.

Sévellec, F., and A. V. Fedorov, 2016: AMOC sensitivity to surface buoyancy fluxes: Stronger ocean meridional heat transport with a weaker volume transport? *Climate Dyn.*, **47**, 1497–1513, https://doi.org/10.1007/s00382-015-2915-4.

Shepherd, A., and Coauthors, 2018: Mass balance of the Antarctic ice sheet from 1992 to 2017. *Nature*, **558**, 219–222, https://doi.org/10.1038/s41586-018-0179-y.

Sloyan, B. M., 2006: Antarctic bottom and lower circumpolar deep water circulation in the eastern Indian Ocean. *J. Geophys. Res.*, **111**, C02006, https://doi.org/10.1029/2005JC003011.

Smedsrud, L. H., and R. Skogseth, 2006: Field measurements of arctic grease ice properties and processes. *Cold Reg. Sci. Technol.*, **44**, 171–183, https://doi.org/10.1016/j.coldregions.2005.11.002.

Stammerjohn, S. E., D. G. Martinson, R. C. Smith, X. Yuan, and D. Rind, 2008: Trends in Antarctic annual sea ice retreat and advance and their relation to El Niño–Southern Oscillation and southern annular mode variability. *J. Geophys. Res.*, **113**, C03S90, https://doi.org/10.1029/2007JC004269.

Storkey, D., and Coauthors, 2018: UK global ocean GO6 and GO7: A traceable hierarchy of model resolutions. *Geosci. Model Dev.*, **11**, 3187–3213, https://doi.org/10.5194/gmd-11-3187-2018.

Sutterley, T. C., I. Velicogna, E. Rignot, J. Mouginot, T. Flament, M. R. Van Den Broeke, J. M. Van Wessem, and C. H. Reijmer, 2014: Mass loss of the Amundsen sea embayment of west Antarctica from four independent techniques. *Geophys. Res. Lett.*, **41**, 8421–8428, https://doi.org/10.1002/2014GL061940.

Swart, N. C., and J. C. Fyfe, 2012: Observed and simulated changes in the Southern Hemisphere surface westerly wind-stress. *Geophys. Res. Lett.*, **39**, L16711, https://doi.org/10.1029/2012GL052810.

——, and ——, 2013: The influence of recent Antarctic ice sheet retreat on simulated sea ice area trends. *Geophys. Res. Lett.*, **40**, 4328–4332, https://doi.org/10.1002/grl.50820.

Swingedouw, D., T. Fichefet, H. Goosse, and M. F. Loutre, 2009: Impact of transient freshwater releases in the Southern Ocean on the AMOC and climate. *Climate Dyn.*, **33**, 365–381, https://doi.org/10.1007/s00382-008-0496-1.

Timmermann, R., and H. H. Hellmer, 2013: Southern Ocean warming and increased ice shelf basal melting in the twenty-first and twenty-second centuries based on coupled ice-ocean finite-element modelling. *Ocean Dyn.*, **63**, 1011–1026, https://doi.org/10.1007/s10236-013-0642-0.

Turner, J., and Coauthors, 2009: Non-annular atmospheric circulation change induced by stratospheric ozone depletion and its role in the recent increase of Antarctic sea ice extent. *Geophys. Res. Lett.*, **36**, L08502, https://doi.org/10.1029/2009GL037524.

——, T. J. Bracegirdle, T. Phillips, G. J. Marshall, and J. S. Hosking, 2013: An initial assessment of Antarctic sea ice extent in the CMIP5 models. *J. Climate*, **26**, 1473–1484, https://doi.org/10.1175/JCLI-D-12-00068.1.

van Aken, H. M., 2007: *The Oceanic Thermohaline Circulation: An Introduction*. Atmospheric and Oceanographic Sciences Library, Vol. 39, Springer-Verlag, 328 pp., https://doi.org/10.1007/978-0-387-48039-8.

Walters, D., and Coauthors, 2019: The met office unified model global atmosphere 7.0/7.1 and JULES global land 7.0 configurations. *Geosci. Model Dev.*, **12**, 1909–1963, https://doi.org/10.5194/gmd-12-1909-2019.

Weaver, A. J., O. A. Saenko, P. U. Clark, and J. X. Mitrovica, 2003: Meltwater pulse 1A from Antarctica as a trigger of the Bølling-Allerød warm interval. *Science*, **299**, 1709–1713, https://doi.org/10.1126/science.1081002.

Weeks, W., 2010: *On Sea Ice*. University of Alaska Press, 664 pp.

Williams, J., and Coauthors, 2016: Development of the New Zealand Earth System Model: NZESM. *Wea. Climate*, **36**, 25–44, https://doi.org/10.2307/26779386.

Williams, K. D., and Coauthors, 2018: The met office global coupled model 3.0 and 3.1 (GC3.0 and GC3.1) configurations. *J. Adv. Model. Earth Syst.*, **10**, 357–380, https://doi.org/10.1002/2017MS001115.

Winsor, P., and G. Björk, 2000: Polynya activity in the Arctic Ocean from 1958 to 1997. *J. Geophys. Res.*, **105**, 8789–8803, https://doi.org/10.1029/1999JC900305.

Yuan, N., M. Ding, J. Ludescher, and A. Bunde, 2017: Increase of the Antarctic sea ice extent is highly significant only in the Ross Sea. *Sci. Rep.*, **7**, 41096, https://doi.org/10.1038/srep41096.

Zunz, V., and H. Goosse, 2015: Influence of freshwater input on the skill of decadal forecast of sea ice in the Southern Ocean. *Cryosphere*, **9**, 541–556, https://doi.org/10.5194/tc-9-541-2015.